ABSTRACT

MAGNETOTRANSPORT IN GaMnAs BASED MICROSTRURCTURES

by Bhim L. Paudel

We present experimental research on magneto-transport at Copper and GaMnAs interface. We report the values of specific contact resistance (ARc) between GaMnAs/Cu interfaces using Circular Transmission Line Method (CTLM) for a wide range of temperature (15K to 290K) above and below Curie temperature (Tc) which is at 145K. Our values of specific contact resistance are very low and close to the order of ~$10^{-8}\Omega cm^2$ which agrees with literature and changes abruptly to close to double of the value at Curie temperature when GaMnAs has phase transition between nonmagnetic to ferromagnetic. We suggest that this arises due to suppression of one of the two spin conduction channels when the phase transition of GaMnAs takes place. We also found the Specific contact resistance has a peak shifted towards lower temperature which suggests the magnetization in the GaMnAs film is suppressed near the Copper interface.

MAGNETOTRANSPORT IN GaMnAs BASED MICROSTRUCTURES

A Thesis

Submitted to the

Faculty of Miami University

in partial fulfillment of

the requirements for the degree of

Master of Science

Department of Physics

by

Bhim L. Paudel

Miami University

Oxford, Ohio

2011

Advisor…….

Dr Khalid F. Eid

Reader……..

Dr Michael J. Pechan

Reader……..

Dr Jan M. Yarrison-Rice

Reader……..

Dr Herbert Jaeger

Table of Contents

List of Tables

List of Figures

ACKNOWLEDGEMENTS

I would like to express my sincere gratitude to my advisor Dr Khalid Eid for his persistent encouragement, careful guidance and support throughout my work and stay in Miami University for two years. Your guideline is not only limited in academics but also extended to my life skill and it is beyond measure. It is my pleasure to find you as my advisor.

I would also like to thank Dr Michael Pechan, Dr Herbert Jaeger and Dr Jan M Yarrision Rice for their invaluable time and suggestions and serving on the advisory committee.

Thanks are due to Michael Eldridge and Mark Fisher for their help and support for the instrumentation and made the work easy to accomplish. I cannot forget the help and cooperation from my friends Calford Otieno, Grant Riley, Robert Tolley, Diana Dahliah and Christopher Brunnet during my work.

I owe special thanks to my wife Parbati for her love, encouragement, and eternal support throughout my academic studies including my research work and beyond. My son Anjal and daughter Enzeela added joy to my research work as they always looked at it with curiosity and became little friends in my work when they got opportunity.

Chapter 1: Introduction

1.1 Electrical Transport in metals

Electrical conduction in non-ferromagnetic metals can be basically explained by the free electron model (also known as the Drude Model)[1]. According to this model, electrons are free to move about the whole metal, like gas molecules in a container, and there is no net motion of electrons in the absence of an electric field, as shown in Figure 1.1 (a). But when an electric field (E) is applied, the electrons have a small drift velocity (v_d) in the direction opposite to the electric field, as shown in Figure1.1 (b). This net drift constitutes the electric current along the field direction. The magnitude of the current is given by:

$$I = neAv_d \qquad (1)$$

where n is the number of free electrons per unit volume, e is the charge of the electron, and A is the cross sectional area of the metal wire.

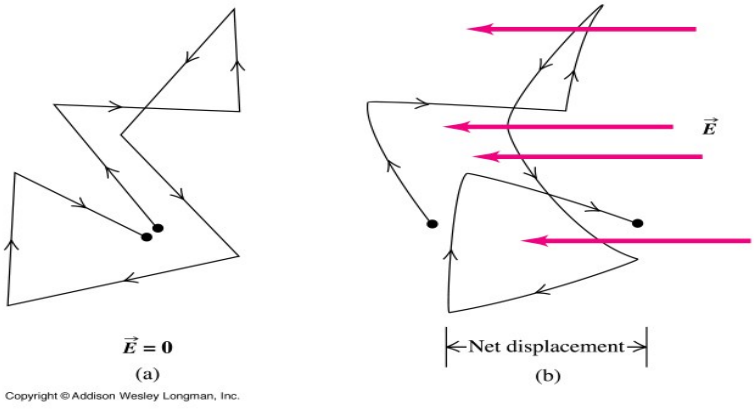

Figure 1.1 Random motion and drift velocity of electrons in a metal

(Source: http://www.google.com/imgres?imgurl=http://www.physics.sjsu.edu/)

Using Newton's second law (F = ma) and $F = eE$ we get,

$$ma = eE$$

$m\frac{\Delta v}{\Delta t}$ = eE which leads to

$v_d = \frac{eE}{m}\tau$, where τ is the average time between collisions of free electrons (2)

Substituting (2) in (1) gives us the current density

$$j = \frac{ne^2\tau}{m}E \quad (3)$$

$$\text{or} \quad j = \frac{E}{\rho} \quad (4)$$

$$\text{where} \quad \rho = \frac{m}{ne^2\tau} \quad (5)$$

In terms of mean free path (λ)

$$\rho = \frac{mv_d}{ne^2\lambda} \quad (6)$$

A more careful quantum mechanical treatment only adds minor modifications, giving

$$\rho = \frac{mv_f}{ne^2\lambda} \quad (7)$$

where v_f is the velocity of electrons at the Fermi Level (energy of highest occupied state).

This shows that the resistivity of a material is inversely proportional to n and λ. In non-ferromagnetic materials both n and λ are the same for spin up and spin down electrons, which means that both "types" of electrons contribute equally to conduction.

1.2 Magnetotransport

The most striking differences between transport in ferromagnetic and non-ferromagnetic materials are that the number of electrons with spin up is different from the number of electrons with spin down, $n^{\uparrow} \neq n^{\downarrow}$, and that the mean free path is spin-dependent, $\lambda^{\uparrow} \neq \lambda^{\downarrow}$ in ferromagnets. This leads to a spin-asymmetric resistivity where $\rho^{\uparrow} \neq \rho^{\downarrow}$. This asymmetry leads, in turn, to a spin polarized electric current $j^{\uparrow} \neq j^{\downarrow}$, where the spin polarization is defined as

$$P=\frac{j\uparrow - j\downarrow}{j\uparrow + j\downarrow} \quad (8)$$

Ignoring spin-flip scattering, conduction in ferromagnetic materials can be explained using a simple model called two current series resistance (2CSR) model[2].

1.3 The Two Current Series Resistance Model (2CSRM)

Conduction of current in a wire can be considered as the combination of two currents due to electrons with spin up, and spin down. In the 2CSRM, these two types of currents do not mix up and flow like two separate channels that are connected in parallel[2]. Despite being a very simple model, the 2CSRM is generally a good approximation when there is very little spin-flip scattering. More involved treatments are needed when there is strong spin flipping in the system[3]. In a normal metal like copper, electrons with spin up and spin down get scattered equally and the two current channels have equal resistivity. But in ferromagnetic materials the two current channels formed by electrons with spin up, and spin down have different values of resistivity due to the different carrier densities and scattering rates.

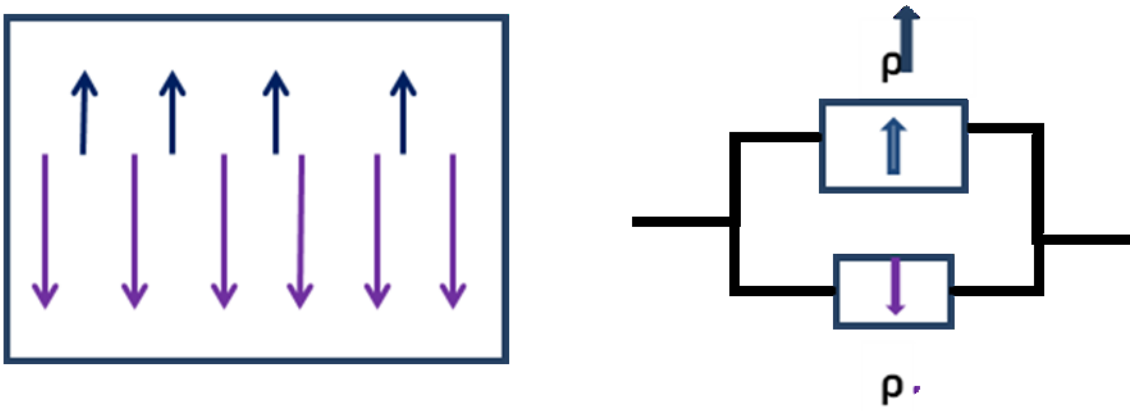

Figure 1.2 Up and down spins in a ferromagnetic material and the corresponding two current channels

For a single ferromagnetic layer, spin asymmetric scattering has no measurable effect. If a multilayer of ferromagnetic (F), non ferromagnetic (N) and ferromagnetic (F) materials is formed, then this effect can produce the giant magnetoresistance (GMR)[4], tunneling magnetoresistance (TMR)[5,6] and spin torque effects[7].

Spin asymmetric scattering in multilayers manifests itself as a difference in the total resistance of the sample when the two ferromagnetic layers are aligned parallel or antiparallel to each other. The two current series resistor model assumes that there are two spin channels conducting current in parallel and the total resistance of each channel is the series sum of the resistances from all the individual layers and interfaces.

1.4 The Ferromagnetic Semiconductor (Ga1-xMnx)As

$(Ga_{1-x}Mn_x)As$ hereafter referred to as GaMnAs, is a ferromagnetic semiconductor and combines properties of ferromagnets and those of semiconductors[8], making it compatible with existing semiconductor technologies. Such a combination can revolutionize the field of spintronics if it leads to actual devices[9]. All our GaMnAs samples are grown by molecular beam epitaxy (MBE), where manganese (Mn) atoms are introduced to the structure of gallium arsenide (GaAs). Mn atoms substitute some of the Gallium atoms and influence the magnetic and transport properties of GaAs significantly[10]. Mn atoms are acceptors that give the free holes and provide the spins that make GaMnAs ferromagnetic. It is a heavily doped P-type semiconductor and typically has charge carrier densities more than 10^{20} per cm^3.The transition temperature at which it loses its ferromagnetic behavior is called the Curie temperature, Tc. The Curie temperature of this material typically ranges from 110K to 190K depending on the percentage of interstitial manganese atoms[11].

1.5 Resistivity measurements

We used the well known Van der Pauw technique[10,12] for resistivity measurements to monitor the annealing process and to check the quality of the samples. This method eliminates the contact and probe resistances by using four probes and can be used for a sample of any arbitrary shape as long as the sample is approximately two-dimensional, piece-wise continuous, and contacts are small and at the periphery of the sample. In this method four electrical contacts are made at the corners of the sample of known thickness (see figure 1.3).

The resistivity of the sample is given by[13]

$$\rho = \frac{\pi}{\ln 2} t \frac{R_{12,34} + R_{23,41}}{2} F \qquad (9)$$

Where $R_{12,34} = \frac{V_3 - V_4}{I_1 - I_2}$ and $R_{23,41} = \frac{V_4 - V_1}{I_2 - I_3}$ and F is the correction factor and is a function of the ratio $R_r = R_{12,34} / R_{23,41}$ that satisfies the relation

$$\frac{R_r - 1}{R_r + 1} = \frac{F}{\ln(2)} \operatorname{arcosh}\left(\frac{\exp[\ln(2)/F]}{2} \right) \qquad (10)$$

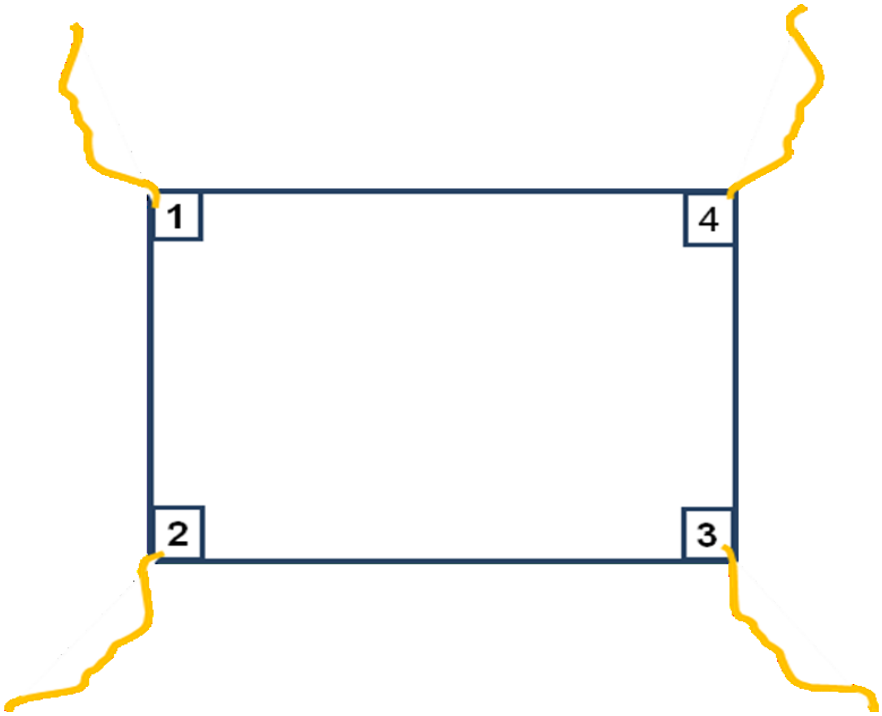

Figure 1.3 Van der Pauw geometry for resistivity measurements

The dependence of R_r with the correction factor F is shown in the figure 1.4

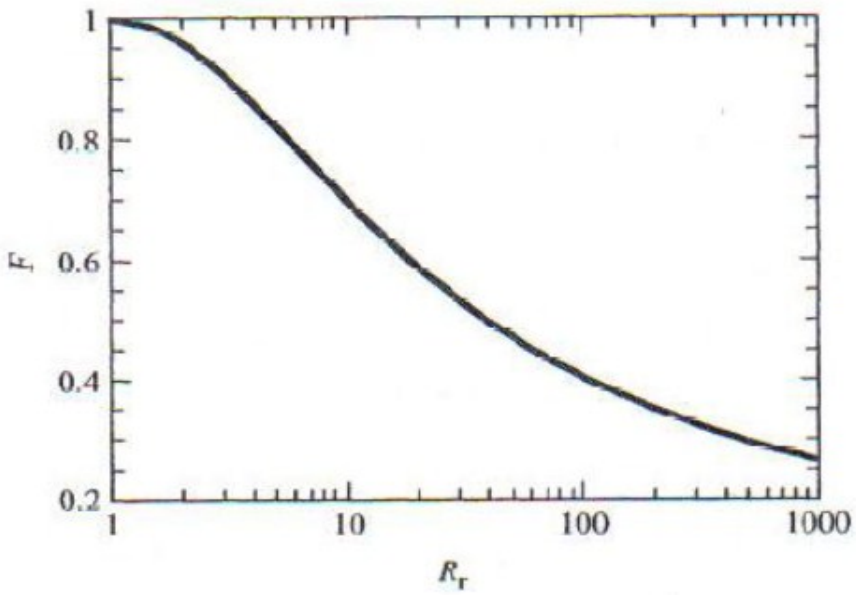

Figure 1.4 Van der Pauw correction factor F vs R_r

For a symmetrical sample such as a circle or a square R_r= 1 and F=1 [12]

1.6 Magnetoresistance

Magnetoresistance is the change in electrical resistance of a sample when a magnetic field is applied. It is the degree of change of resistance produced due to magnetic field in comparison to the resistance without magnetic field. Magnetoresistance ratio (MR) is given by

$$MR = \frac{\Delta R}{R_0} = \frac{R_H - R_0}{R_0} \qquad (11)$$

where R_0 and R_H represent the resistance of the material without applying magnetic field and with magnetic field, respectively.

There are three well known types of magnetoresistance. Anisotropic magnetoresistance (AMR) which is the effect of anisotropic change of electrical resistance in response to the rotation of the magnetization relative to the electrical current and it appears due to the anisotropic scattering cross section of conduction electrons depending on whether they

travel along or perpendicular to the magnetization[14]. Tunneling magnetoresistance (TMR) that occurs in magnetic tunnel junctions which is a component consisting of two ferromagnets separated by a thin insulator through which electrons can tunnel form one ferromagnet to another[15]. This effect is observed through quantum mechanical tunneling of electrons across the insulating layer. Giant magnetoresistance (GMR) is the change in resistance (usually large) in a multilayer composed of a non ferromagnetic material sandwiched between two ferromagnetic materials and depends on the relative direction of the magnetization of the ferromagnetic layers. It is usually low if the magnetizations of the ferromagnetic layers are parallel (i.e. pointing in the same direction), but usually high

when the magnetizations of the two ferromagnetic layers are anti-parallel to each other.

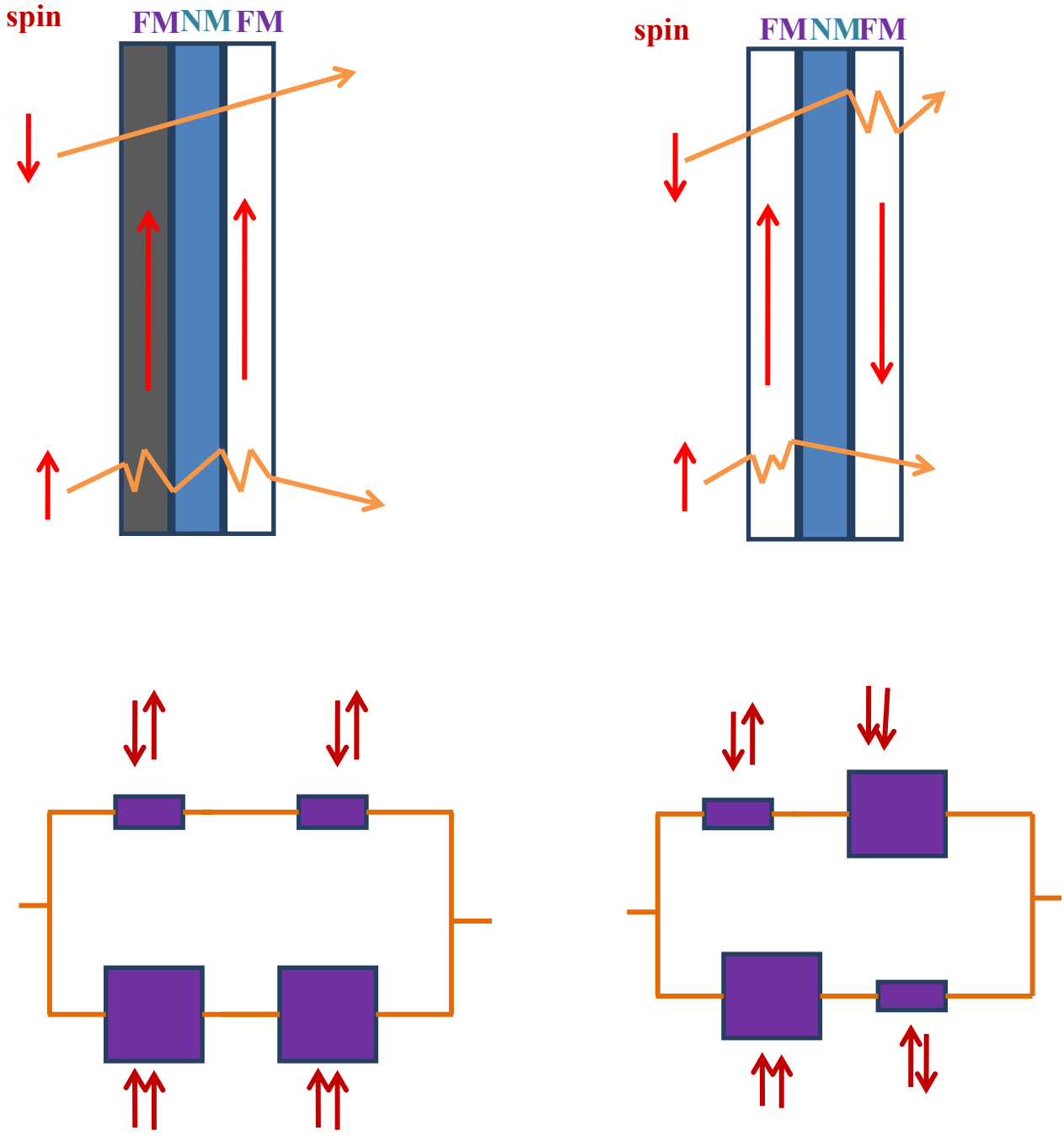

Figure 1.5 Ferromagnetic layers with parallel and antiparallel magnetization

1.7 About this thesis

This thesis aims to study the contact resistance between the heavily doped ferromagnetic P-type semiconductor GaMnAs and normal metal copper. More specifically, the thesis will address the temperature variation of the contact resistance, especially at the Curie temperature when GaMnAs becomes ferromagnetic. Of particular interest to this thesis is to observe any potential effect associated with spin filtering at the GaMnAs/Cu interface when GaMnAs becomes ferromagnetic. I describe the micro fabrication process that utilizes photolithography and metal deposition onto GaMnAs to create the microstructures used in the studies. And then report our results for the contact resistance between GaMnAs and Copper using Circular Transmission Line Method (CTLM).

Chapter 2: Contact Resistance

2.1 Introduction

Any electrical current from the outside world is circulated into a real semiconductor device through a contact. There can be semiconductor- semiconductor or metal-semiconductor contacts. We are concerned with metal-semiconductor contacts. Every contact introduces a significant resistance to the bulk metal and bulk semiconductor resistance which mostly depends on the resistance of the contact material. So, studying the contact resistance is very important for efficient semiconductor devices. When a metal and a semiconductor (or even two different metals) are brought into contact, there will be an additional resistance at the interface between the two layers and a thin portion of the semiconductor gets depleted of charge carriers. This charge-depleted zone can lead to current-rectifying effects giving the metal-semiconductor diode (or Schottky diode). This behavior occurs when the semiconductor layer has low to moderate doping density. The conduction process across such barriers occurs through thermionic emission, where charge carriers will move across the barrier only if they are given enough energy through an applied voltage or through thermal energy[16]. However, if the doping density is extremely high (10^{21}per cm^3), the charge-depleted zone will be so thin that it is more likely for electrons to tunnel through the barrier without needing energy to jump over it. Furthermore, this tunneling probability is basically independent of the sample temperature and leads to a non-rectifying (i.e. linear) current-voltage behavior.

The metal-semiconductor contact was first discovered and studied by Braun in 1874[17] to explain the current transport in Metal Sulfides. Its first acceptable theory was developed by Schottky in 1930[18]. There are two types of metal-semiconductor contacts. The first one is the rectifying contacts, or Schottky contacts, in which charge flows in one direction but not the other. This type of contact is the basis for Schottky diodes. Second type of contacts is ohmic contacts which have linear current-voltage characteristics in

which charge flows in both directions without rectification[19]. Ohmic contact resistance needs to be minimized in semiconductor devices.

2.2 Metal-Semiconductor Contacts

Metal-semiconductor contacts fall into two basic categories. The current flows either in plane and normal into the contacts (fig 2.1). Vertical and horizontal contacts have different effective area from the true contact area and may behave differently.

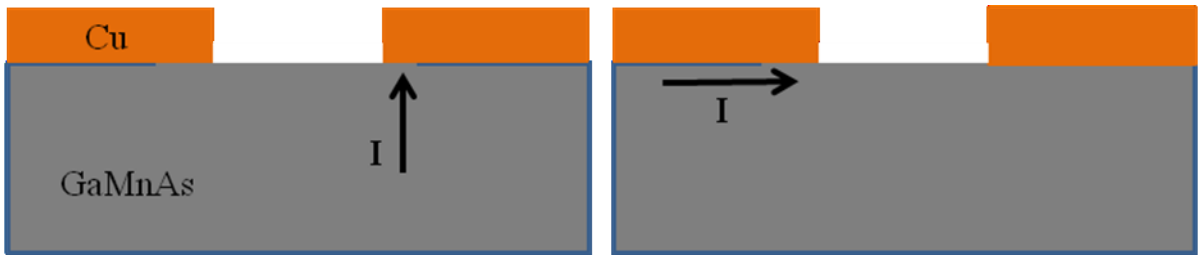

Figure 2.1 Flow of Current through normal contact and in plane contact

When metal is lying on semiconductor and making ohmic contacts to an n-type layer in a p-type substrate the total resistance R_T between end points of the sample can be divided into three components namely the resistance of the metallic conductor $R_{m,}$ the contact resistances R_c, and the semiconductor resistance $R_{s.}$

So the total resistance is

$$R_T = 2R_m + 2R_c + R_s \qquad (2.1)$$

The semiconductor resistance is determined by the sheet resistance of the n-layer. The contact resistance is usually multiplied by the contact area between the metal and semiconductor giving the "intrinsic" quantity called the specific contact resistance (ARc).

2.3 Transfer length (L_t)

Current always chooses the path of least resistance. If current is passed through a metal semiconductor contact region, the path of the current includes a portion of the metal

immediately above the metal-semiconductor interface where there is current crowding effect. The transfer length (L_t) is the distance over which most of the current transfers from the semiconductor into the metal or from the metal into the semiconductor (fig 2.2). It is on the order of 1 μm or less.

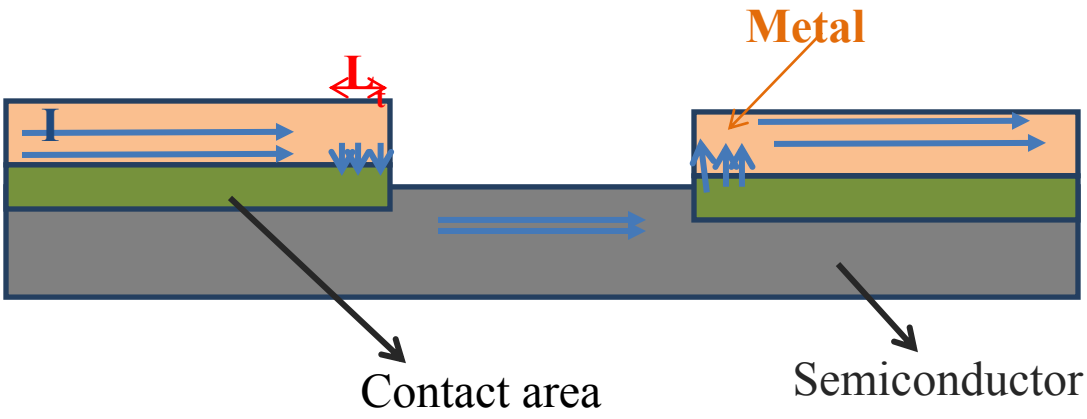

Figure 2.2 Side view of metal semiconductor contact showing current flow through the path of least resistance

We use the circular transfer length method (CTLM) to measure the specific contact resistance between the contact interfaces. It was originally proposed by Shockley[20]. This method helps to eliminate the current crowding from one contact to another[21]. We use the typical CTLM layout proposed by Marlow and Das[22] because it takes single step for fabrication. It consists of a circular contact, which is separated from the surrounding metal by a ring-shaped gap on the semiconductor. The structure has a series of circles with increasing gap for the constant internal diameter. The layout pattern is shown in figure 2.3.

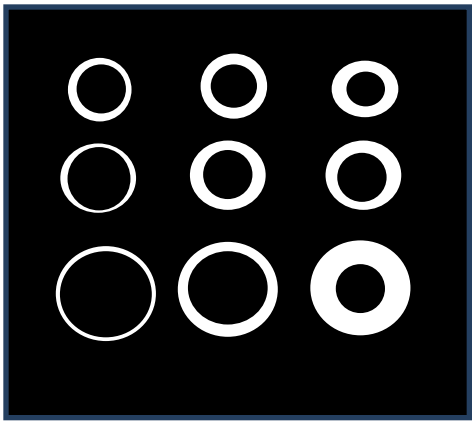

Figure 2.3 Top view of CTLM structure

For circular patterns consisting of a conducting circular inner region of radius r, a gap of width w, and a conducting outer region of inner radius (r + w) as shown in fig 2.4. The total resistance between the internal and the external contacts is given by[23,24]

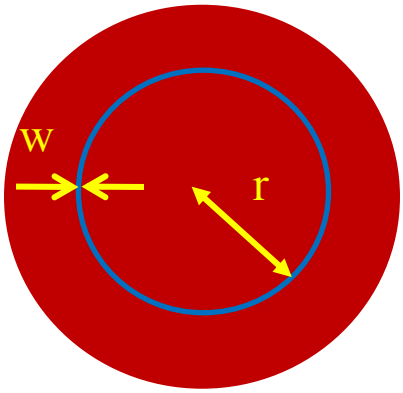

Figure 2.4 Circular contact resistance test

$$R_T = \frac{\rho}{2\pi t}\left[\frac{L_T}{r}\frac{I_o\left(\frac{r}{L_T}\right)}{I_1\left(\frac{r}{L_T}\right)} + \frac{L_T}{r+w}\frac{K_o\left(\frac{r}{L_T}\right)}{K_1\left(\frac{r}{L_T}\right)} + ln\left(1+\frac{w}{r}\right)\right] \quad (2.2)$$

Where ρ is the resistivity of the semiconductor, L_T is the transfer length, and I_i and K_i denote the modified Bessel functions of the first order. For $r >> 4L_T$, the Bessel function ratios Io / I_1

and K_0/K_1 tend to unity and the total resistance becomes

$$R_T = \frac{\rho}{2\pi}\left[\frac{L_T}{r} + \frac{L_T}{r+w} + ln\left(1 + \frac{w}{r}\right)\right] \quad (2.3)$$

In the circular transmission test structure, r >> w, and the equation (2.3) simplifies to

$$R_T = \frac{\rho}{2\pi rt}(w + 2L_T) \quad (2.4)$$

where C is the correction factor and it is given by

$$C = \frac{r}{w} ln\left(1 + \frac{w}{r}\right)] \quad (2.5)$$

Calculation of Specific Contact Resistance (AR_c)

Knowing the value of Transfer length (L_T), thickness and resistivity of the material the specific contact resistance can be calculated by using the expression

$$L_T = \sqrt{\frac{AR_c t}{\rho}} \quad (2.6)$$

2.5 Sample preparation

GaMnAs samples we use are grown mainly by molecular beam epitaxy (MBE) at Notre Dame University. During this process, manganese (Mn) atoms introduced to the structure of GaAs. The percentage of Mn atoms introduced influences the magnetic and transport properties of GaMnAs. So it is not ready to use immediately after it is grown. We need to go through the following process before we use it to make features for our contact resistance measurements.

2.5.1 Annealing

During the growth of GaMnAs, some gallium atoms are substituted by manganese atoms. Such Mn atoms are called substitutional atoms and are responsible for generating the holes and the ferromagnetism. Yet, some Mn atoms end up landing in places between lattice sites and are called interstitial atoms (Mn_I). Contrary to Mn atoms, the Mn_I atoms are acceptors that compensate the holes, diminish ferromagnetic order and make the

crystal dirtier. Studies show that Curie temperature can be improved by post growth annealing at temperatures close to the growth temperatures.[25] Temperature above the growth conditions destroys the lattice structure of the semiconductor. When we heat the sample, manganese atoms in the lattice gain high kinetic energy and move to the surface, where they are passivated by bonding to oxygen and/or nitrogen and no longer remain as interstitial atoms. This increases the purity of crystal structure and reduces the resistivity. Furthermore it increases the Curie temperature of GaMnAs, a requirement for spintronics.

2.5.2 Photolithography

Photolithography is the process of transferring the image of suitable mask patterns onto a thin layer of photosensitive material that covers a semiconductor wafer. The steps involved in photolithography are given below.

2.5.2.1 Surface Treatment

In this process we clean the surface to remove dust and any dirt that will disrupt the photolithography. The properties of metal/semiconductor interface are altered significantly due to organic compounds. We first clean the sample with de-ionized water, then soak our sample in acetone and use ultrasonic agitator to remove the organic compounds. The sample is then rinsed well with isopropyl alcohol (IPA) and flushed with dry nitrogen. This process is done inside the cleanroom in which the dust particles in air are tremendously reduced so that the sample surface is free from any kind of foreign bodies.

2.5.2.2 Resist Coating

Resist coating is the process of spinning a thin layer of resist (photosensitive polymer) on a wafer on which the patterns are to be transferred. We use lift off resist (LOR) which is a mixture of cyclopentanone and Propylene Glycol Methyl Ether. A positive photoresist S1813 (1:1) thinner is used as a photoresist. It is a mixture of electronic grade propylene glycol monomethyl ether acetate, mixed novolak resin,cresol, diazophotoactive

compound fluroaliphatic polymer esters. Two drops of resist is put on the wafer spreads uniformly on the surface as the spinner rotates. The thickness of layer is controlled by the frequency of rotation of the wafer in the spinner. The speed is more for more viscous resist. For LOR we use spinning speed 300 rpm and for photoresist we use 4000 rpm for 40 seconds. We use Laurell Spinner Model WS400B-6NPP/LITE (fig 2.5) for this process.

Figure 2.5 Laurell Spinner Model WS400B-6NPP/LITE

2.5.2.3 Writing patterns on the sample

The resist coated sample is transferred to a mask aligner (fig 2.6). We use masks with circular pattern. UV Light is directed through the mask and onto the resist-coated sample which is held in direct contact to the mask. We expose the sample with UV light for 40 seconds. The wafer is immediately transferred into developing solution (CD26) and soaked for 30 seconds and washed well with DI water to stop developing and flushed with dry nitrogen. Figure 2.6(b) shows the patterned sample obtained after

photolithography.

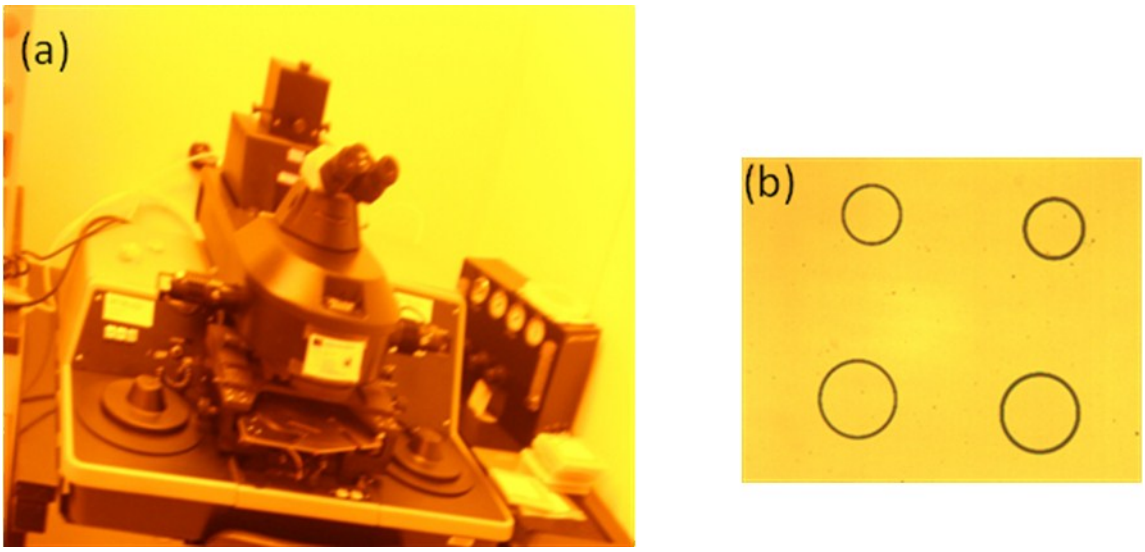

Figure 2.6 (a) Mask aligner (Myriad Semiconductor) (b) Patterns on sample

2.5.2.4 Stripping photoresist and oxide from the surface

Before metal deposition the sample needs further cleaning to rid of the photoresist residues that may still have been present on the wafer surface. We use two etching process namely oxygen plasma etching and wet etching to remove the photoresist on the surface of the sample.

2.6 Oxygen Plasma etching

In this process the wafer is placed in oxygen plasma. Low energy below the atomic displacement threshold ensures that the lattice of the sample is not affected.[26] Ionized oxygen atoms hit the sample of the surface and oxidize the outer layer of photoresist which turns into gas and gets sucked out by vacuum system. We etch our sample for 20 seconds using a Plasma Etch, PE50 (Fig 2.7).

Figure 2.7 Oxygen Plasma etch PE50Wet Etching

To remove the native oxides formed on the surface of sample we use etching solution which is a mixture of sulfuric acid and water (ratio 2:1000). The sample is transferred into etching solution after oxygen plasma etching. We etch the sample for 20 seconds and rinse well with DI water. The sample is then immediately loaded into vacuum chamber for metal deposition and pumped down quickly so that the sample is protected from formation of any oxide, and dust settling on it.

2.7 Metal Deposition

We deposit copper on the sample in a background pressure about 2×10^{-7}mbar using a custom-built compound vacuum chamber (Figure 2.8). The thickness of copper deposited is 140nm. The copper contacts were circular discs with inner diameter ranging from 200µm to 600µm separated from an outer copper structure by a circular gap of nominal width varying from 3µm to 80µm.

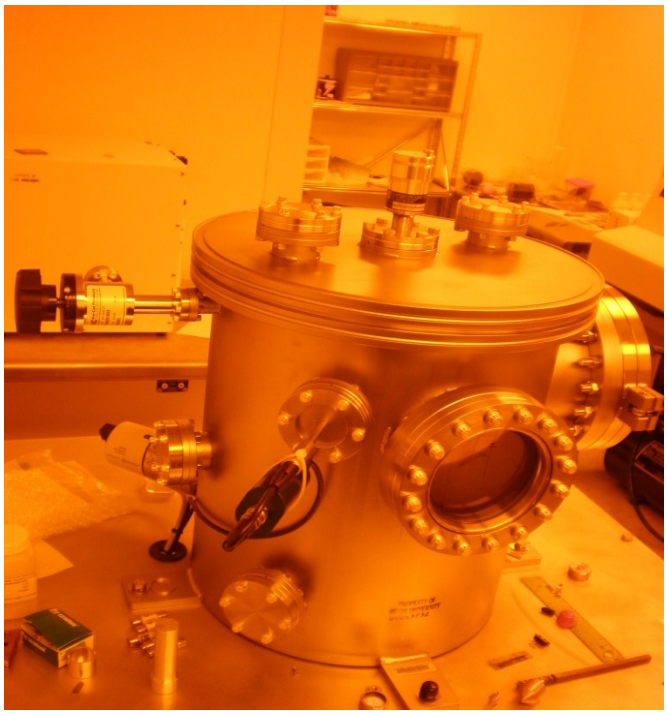

Figure 2.8 Metal deposition Chamber

2.8 Lift off

After deposition of metal, the sample is put into acetone for about 10 minutes to dissolve the resist below the metal layer. We use an ultrasonic agitator to clean the sample if necessary. We get clean rings of GaMnAs after this process.

2.9 Summary of actual steps for sample preparation

- Cleave the wafer to get a piece of an approximate size of 10mm by 5mm.
- Anneal the sample at 180°C for 92 hrs.
- Clean the sample with DI water, and then soak into acetone for 2 minutes. Use ultrasonic agitation for a minute and rinse well with isopropyl alcohol (IPA) and dry with nitrogen.
- Load the sample on the spinner and put the vacuum on. Add few drops of lift of resist (LOR) on it and spin @3000rpm for 40 seconds.
- Bake the sample for 10 minutes at 150°C.

- Cool the sample and load it again on the spinner and put few drops of photoresist (S 1813 1:1 thinner) on it and spin @4000 rpm for 40 seconds.
- Bake the sample for 1 minute at 105°C.
- Load the mask in the mask aligner. Align the sample to the features to be written and expose UV light for 4.6 seconds.
- Develop the sample for 40 second in developer (CD 26) and rinse well with De ionized water to stop developing and dry with nitrogen.
- Load the sample into oxygen plasma etching chamber and etch for 20 seconds which removes organic solvents and unwanted resist layers on the surface of the sample.
- Attach the sample on a copper block using a tiny drop of photoresist and warm it so that the sample sits well on the block.
- Prepare etching solution H_2SO_4: H_2O in the ratio of 2:1000 and etch the sample for 20 seconds that removes the native oxides on the surface. Then transfer the sample into DI water to stop etching. Remove excess water on the block and sample.
- Load the sample with the copper block quickly into the metal deposition chamber and pump it down.
- Deposit copper when the pressure in the chamber reaches to about 2×10^{-7}mbar. The thickness of the metal deposited is calculated from the reading of film thickness monitor. We deposit about 140nm of copper.
- Take the sample out and put into acetone for about 10 minutes to lift off resist so that the sample detaches from the copper block. Apply ultrasonic agitation for few seconds to clean the residues on the surface of the sample.
- Dry the sample with nitrogen.
- Now the sample is ready for measurement.
- We measured the internal diameter of the circles and the gaps between the inner and outer circles using Field Emission Scanning Electron Microscope. The SEM images of the actual samples are shown in figure 2.9 (a) and 2.9(b).

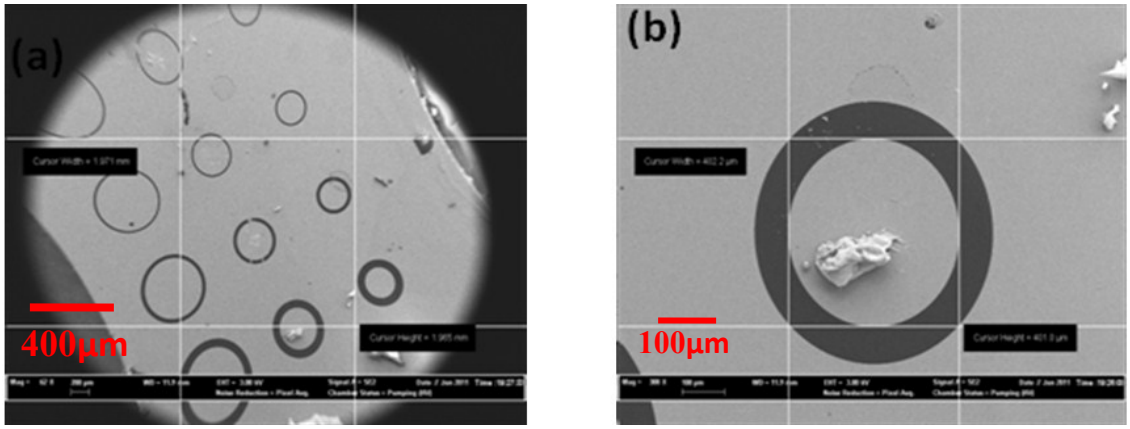

Figure 2.9 (a) SEM image of patterns (b) SEm image of a circular feature

2.8: Resistance Measurements

We fix the sample on the custom-made cryostat head and use a four probe method to measure the resistance. We connect two wires at the inner circle of the feature and two wires to the outer metal terminal using indium soldering (Figure 2.10). Current flows from the inner disk to the outer metal terminal through the gap of GaMnAs and the voltage is measured across the inner disk and outer terminal. We apply a constant current of 10 µA for our measurement. Voltage and current is controlled by using a lock-in amplifier. The sample is cooled to 20K using a closed cycle helium cryostat and then warming up to the room temperature.

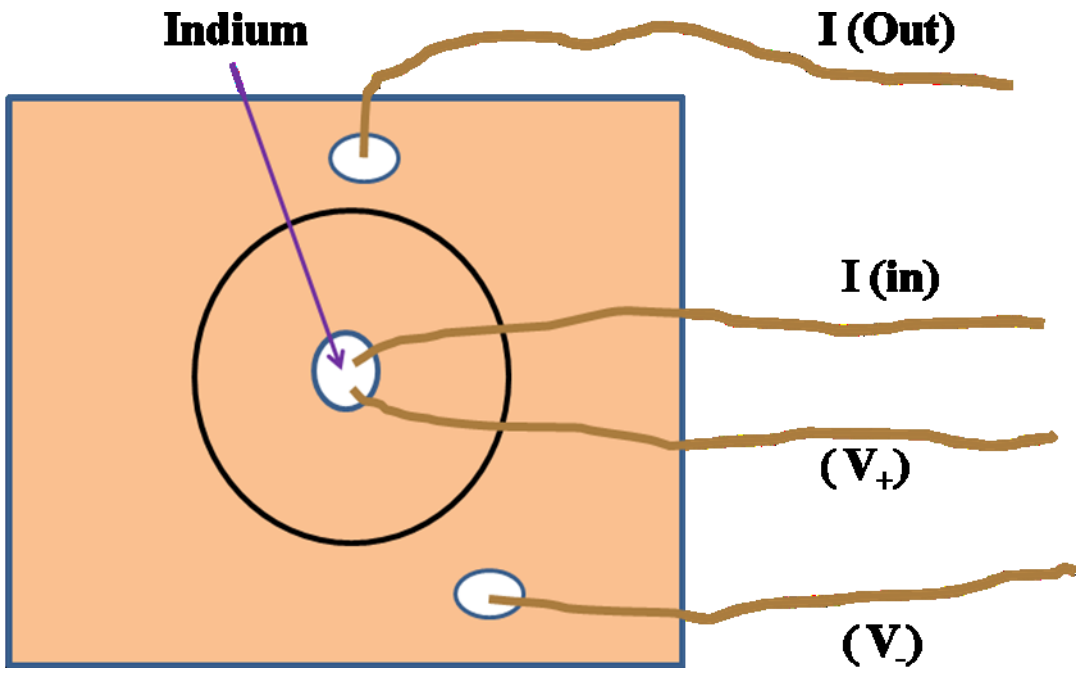

Figure 2.10 Connection of wires in the sample

We record the data of variation of net resistance with temperature using LabVIEW program. The resistance is found to have a peak value at the transition temperature Tc (Figure 2.11)

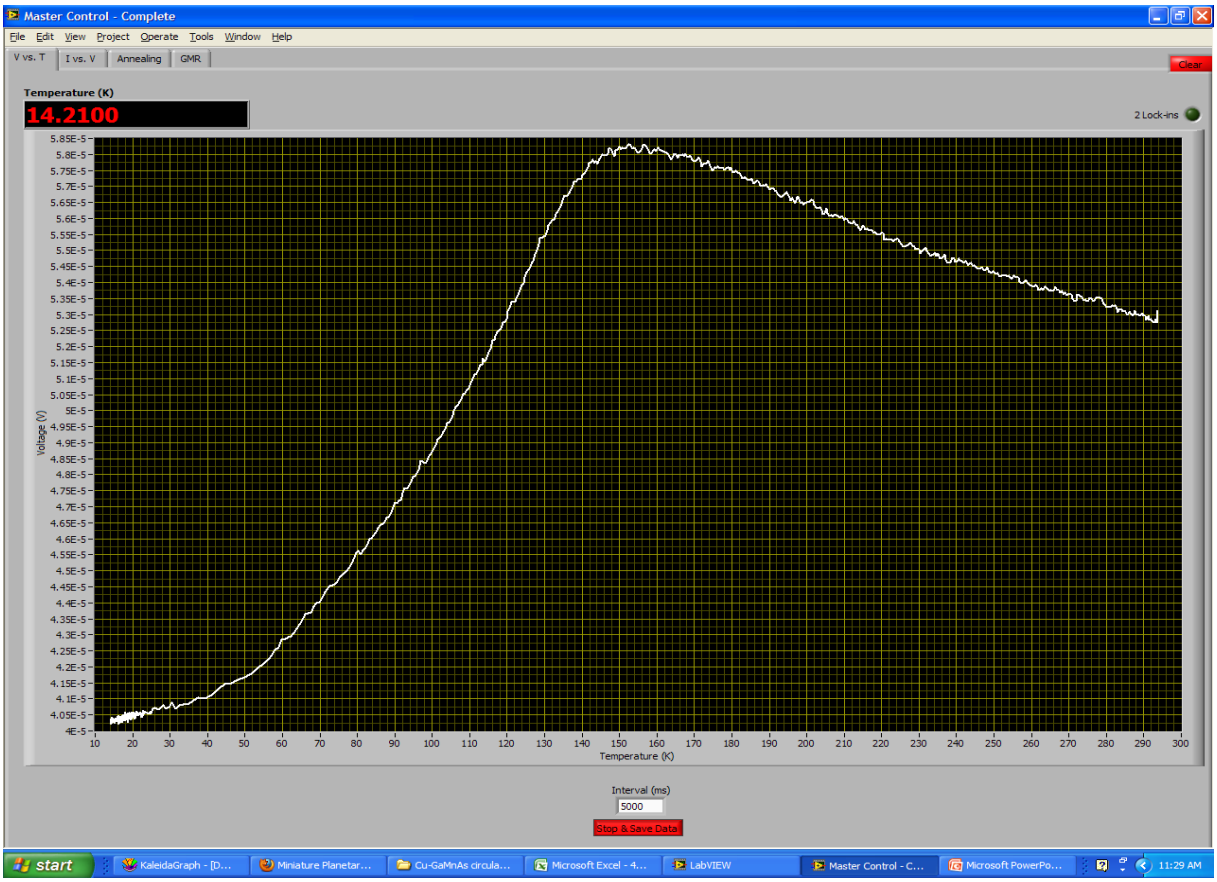

Figure 2.11 Variation of net resistance with temperature

Chapter 3: Result and Discussion

We started with the sample 100324 A with 100nm GaMnAs thickness. We measured the resistance of the sample lowering its temperature. The temperature at which the resistance decreases rapidly gives us the Curie temperature. The Curie temperature is improved with increase in annealing time as the interstitial manganese atoms escape from the lattice structure. For the sample as grown Curie temperature was about 50K while for the sample annealed for 92 hours at 180°C its value increased to 145K.

Figure 3.1 displays the dependence of the current in the device on the applied D.C. voltage showing a linear Ohmic behavior without rectifying properties. The doping density of GaMnAs is so high ($\sim 10^{21}$ per cm^3) is so high that the depletion zone at the GaMnAs/copper interface is extremely thin (~1nm), allowing for efficient carrier tunneling and leading to a low resistance Ohmic behavior. Since the interface has no rectifying effects, a standard and low frequency lock-in technique with a low bias current $\leq 10\mu A$ was used to measure the resistance of the devices in zero applied magnetic fields[27].

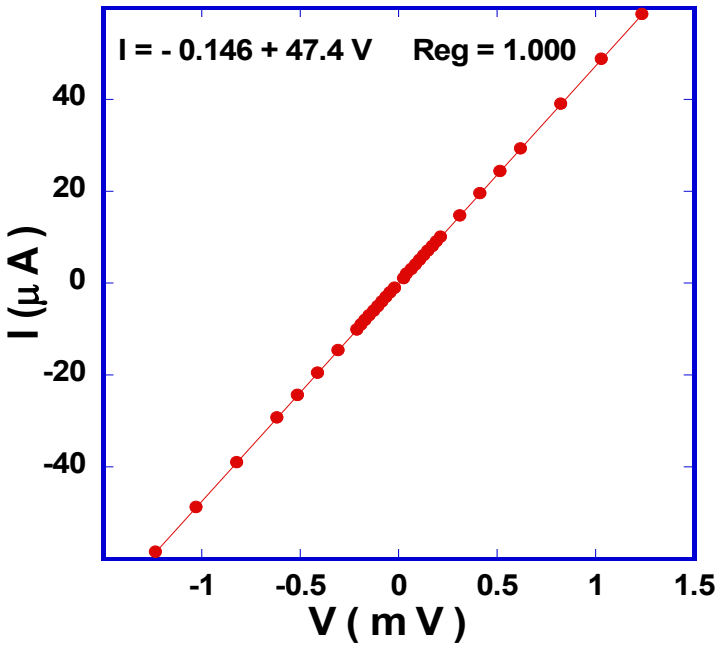

Figure 3.1 Current-voltage variations at interface of Cu and GaMnAs

In order to find the specific contact resistance at first we measured the total resistance R_T that includes resistances at the contact interfaces and the sheet resistance of GaMnAs for features of various gaps (w) at different temperature. Figure 3.2 shows those values for features with gaps 8μm, 10μm, 15μm, 40μm. We then picked up resistances at specific temperatures for different gaps as shown by the vertical lines in the figure.

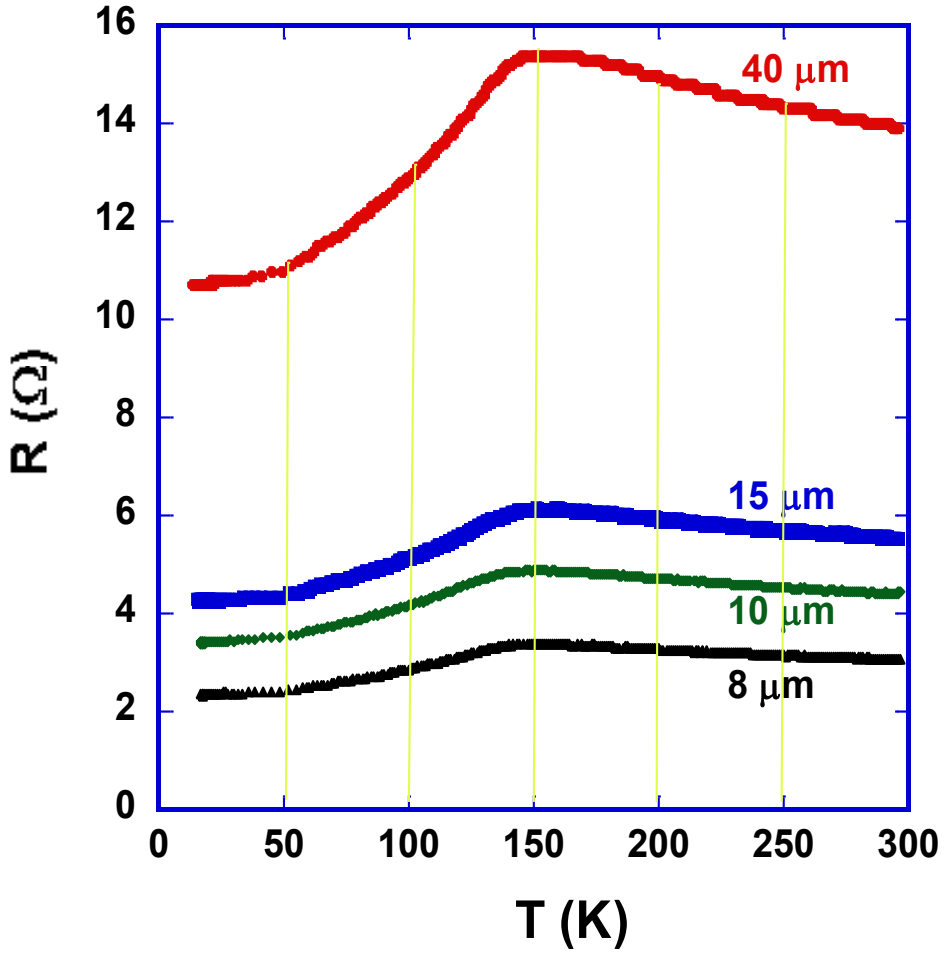

Figure 3.2 Variation of resistance with temperature at different gaps

We then plot the width (w) and resistance and get the slope and intercept of the lines for different temperatures. The typical plots are shown below in figure 3.3 in which the factor f represents $2\pi tr/C$ with t as the thickness of GaMnAs, r the inner radius of the circular disc, and C is the correction factor.

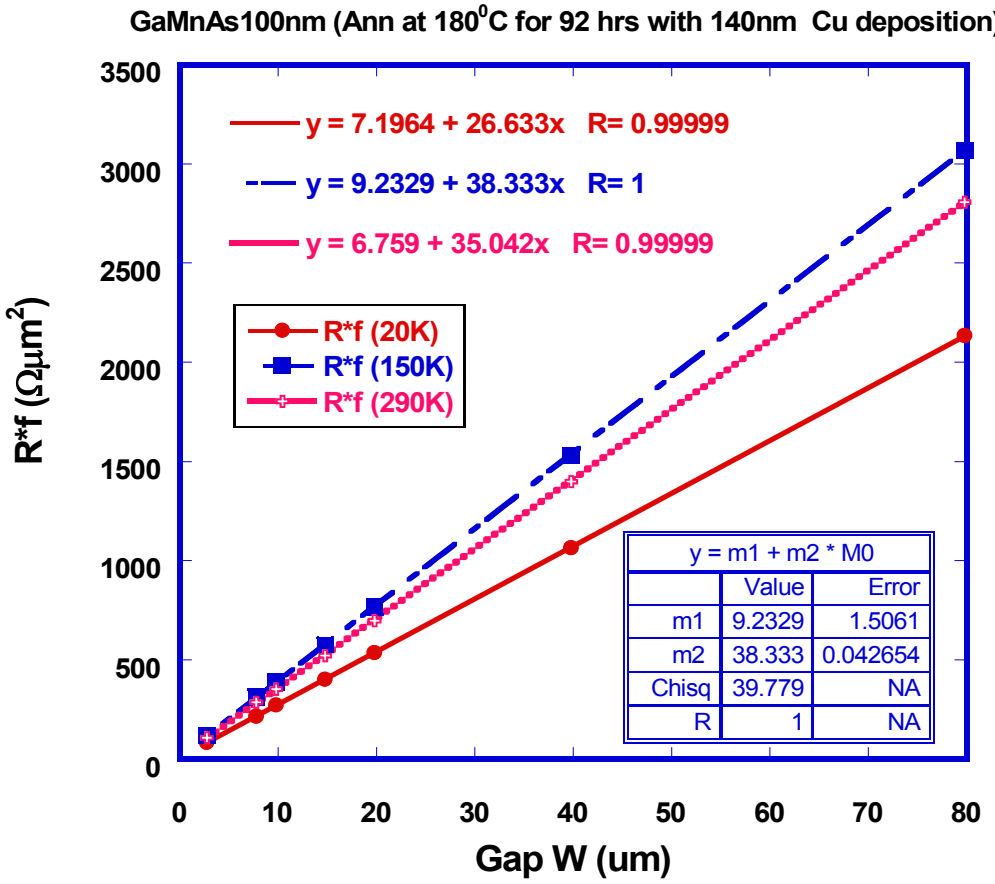

Figure 3.3 Variation of R*f with gap (w) and the error in slope and intercept

Rewriting the equation 2.4 and 2.5

$$R_T = \frac{\rho}{2\pi rt}(w + 2L_T)C \quad = \quad \frac{\rho(w+2L_T)}{f} \tag{2.4}$$

$$C = \frac{r}{w}\ln\left(1 + \frac{w}{r}\right) \tag{2.5}$$

From equation (2.4) we see that slope of the plot of " R_T *f" Vs "w " gives the resistivity (ρ) of the semiconductor and the transfer length can be calculated from the intercept.

The correlation coefficient of the data points as shown in the figure 2.3 is almost 1 and it confirms that the data are well correlated to each other. The error on slope is much less than 1% while the error in intercept is about 10%.

Table 1 shows the calculated values of resistivity and transfer length at various temperatures and further analysis for specific contact resistance (ARc)

Table 3-1 Calculated values of resistivity, transfer length and ARc

Temp (K)	**Slope (Ω μm)**	**Intercept (Ω μm^2)**	**Resistivity (mΩcm)**	**Lt (μm)**	**ARc (Ω cm^2)**
20	269.93	173.55	2.6993	0.32147	2.79E-07
30	271.97	178.55	2.7197	0.32825	2.93E-07
40	274.81	181.74	2.7481	0.33066	3.00E-07
50	278.83	188.03	2.7883	0.33718	3.17E-07
60	284.76	199.97	2.8476	0.35112	3.51E-07
70	292.03	210.43	2.9203	0.36029	3.79E-07
80	301.18	229.21	3.0118	0.38052	4.36E-07
90	311.88	231.13	3.1188	0.37054	4.28E-07
100	322.72	253.33	3.2272	0.39249	4.97E-07
110	336.8	263.12	3.368	0.39062	5.14E-07
120	350.72	283.6	3.5072	0.40431	5.73E-07
130	368.12	296.92	3.6812	0.40329	5.99E-07
140	384.29	292.27	3.8429	0.38027	5.56E-07
150	391.52	262.65	3.9152	0.33542	4.40E-07
160	391.63	257.34	3.9163	0.32855	4.23E-07
170	389.77	249.22	3.8977	0.3197	3.98E-07
180	387.31	241	3.8731	0.31112	3.75E-07
190	384.18	237.08	3.8418	0.30855	3.66E-07
200	380.61	234.47	3.8061	0.30802	3.61E-07
210	377.52	229.63	3.7752	0.30413	3.49E-07
220	371.03	278.21	3.7103	0.37492	5.22E-07
230	368.16	271.83	3.6816	0.36917	5.02E-07
240	365.17	270.73	3.6517	0.37069	5.02E-07
250	362.04	274.19	3.6204	0.37867	5.19E-07
260	358.96	298.93	3.5896	0.41638	6.22E-07
270	357.46	284.23	3.5746	0.39757	5.65E-07
280	356.02	275.76	3.5602	0.38728	5.34E-07
290	352.41	284.38	3.5241	0.40348	5.74E-07

3.1 Variation of resistivity with temperature

Above Curie temperature GaMnAs is non magnetic and the resistivity is dominated by the bulk GaMnAs contribution and follows general characteristics of a semiconductor. Our result (figure 3.4) shows that the resistivity decreases at a slower rate above the Curie temperature but below the Curie temperature the slope is steeper and the resistivity decreases at a faster rate with GaMnAs in the ferromagnetic state which is expected.

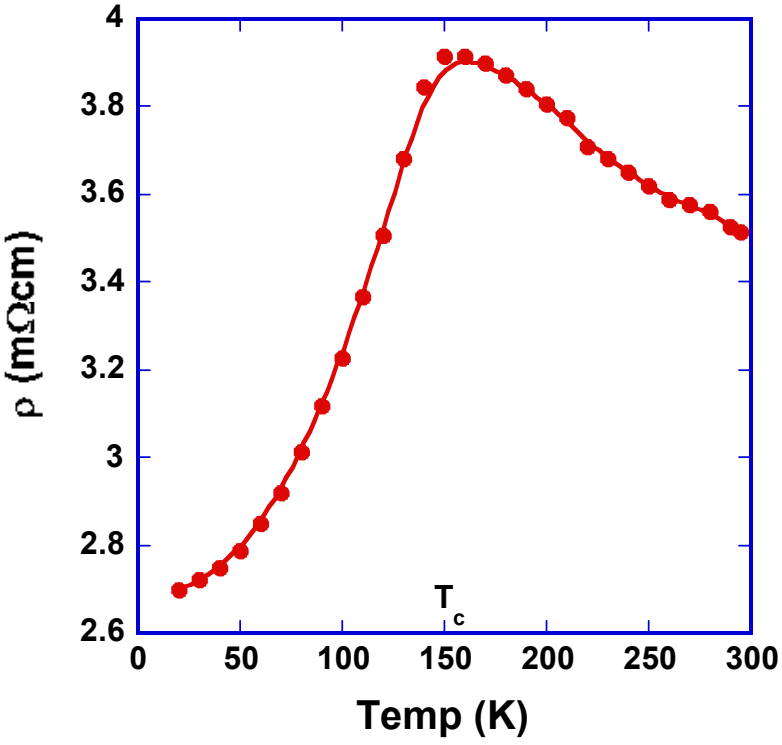

Figure 3.4 Variation of resistivity with temperature

3.2 Variation of ARc with temperature

The specific contact resistance as a function of temperature is shown in the figure 3.5. Contact resistance decreases slowly with decrease in temperature but when it reaches the Curie temperature there is an abrupt rise and it roughly doubles .This large rise in contact resistance is clearly caused by the ferromagnetic order in GaMnAs and may indicate that either spin up or spin down channels of conduction have been suppressed below T_c. Apart from the discontinuity,

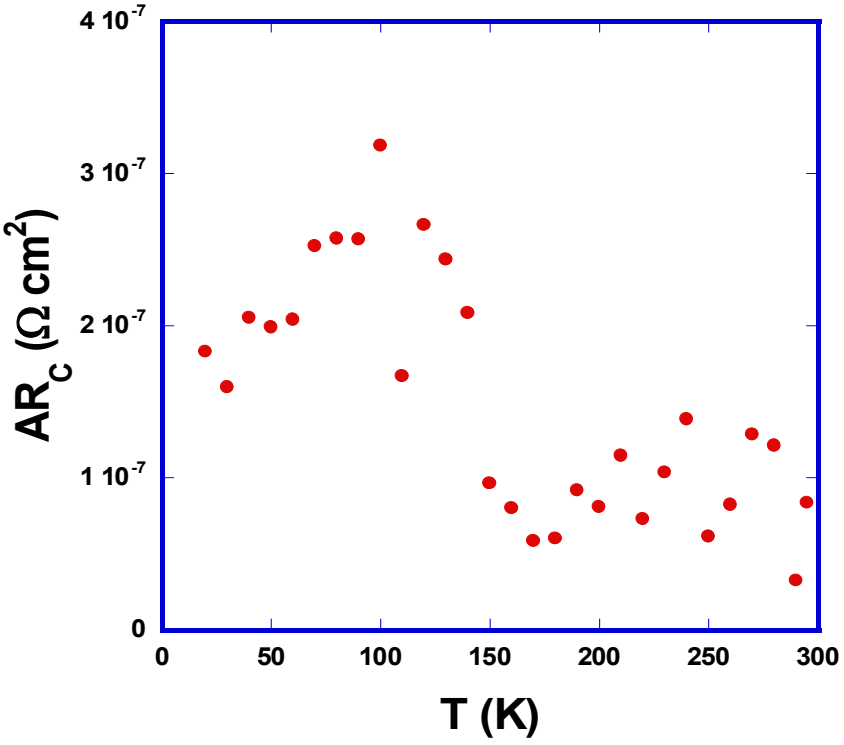

Figure 3.5 Variation of ARc with temperature

AR_c decreases slowly with decreasing temperature, which indicates that the current conduction mechanism at the interface is tunneling and not thermionic emission. A second possible cause of decreasing AR_c might be the presence of metal shunts at the surface states[28]. Our data is not sufficient to distinguish between these two possibilities.

Below T_c, the initial increase of AR_c with decreasing T may be due to increase in spin polarization[29,]. Spin polarization in copper takes place by Zener tunneling of polarized electrons between the valence band of GaMnAs and the conduction band of copper.

Above the Curie temperature of GaMnAs both the spin-up and spin-down electrons have equal tunneling probabilities, while below T_c one of the spin channels is likely to be suppressed. Assuming that the tunneling probability of the other channel remains the same, the total current density will then be reduced, leading to increase in AR_c. Such increase of AR_c can therefore give an estimate of the spin polarization at the interface. In fact, the doubling of AR_c ,we observed suggests a significant spin polarization, close to 100% , although the scatter of the data does not allow us to make an accurate quantitative estimate. Furthermore, we cannot ignore the possibility that both the spin-up and the spin-down bands in GaMnAs may shift at T_c, which can result in a further modification of AR_c. This may explain why our observed value of AR_c doubles around T_c. Such large polarization is generally in agreement with values found in experiments on Esaki diode[3].

3.3: Transfer length

We found the transfer length L_T smaller than 0.5μm for all studied temperatures (Fig 3.6), showing that the assumption $L_T/w << 1$ is justified. The form of the dependence of L_T on temperature is somewhat similar to that of AR_c because $L_T = \sqrt{\frac{AR_c t}{\rho}}$ which clearly indicates that when the values of AR_c are small relative to the sheet resistance of the semiconductor, the transfer length will also be small. The value that we found for AR_c is about $1\times10^{-7}\Omega cm^2$, which is quite small, comparable to the values found using carefully designed alloyed contacts, where alloying creates a large doping density at the interface, thus leading to low contact resistance values.[30,31] It is according to our expectation.

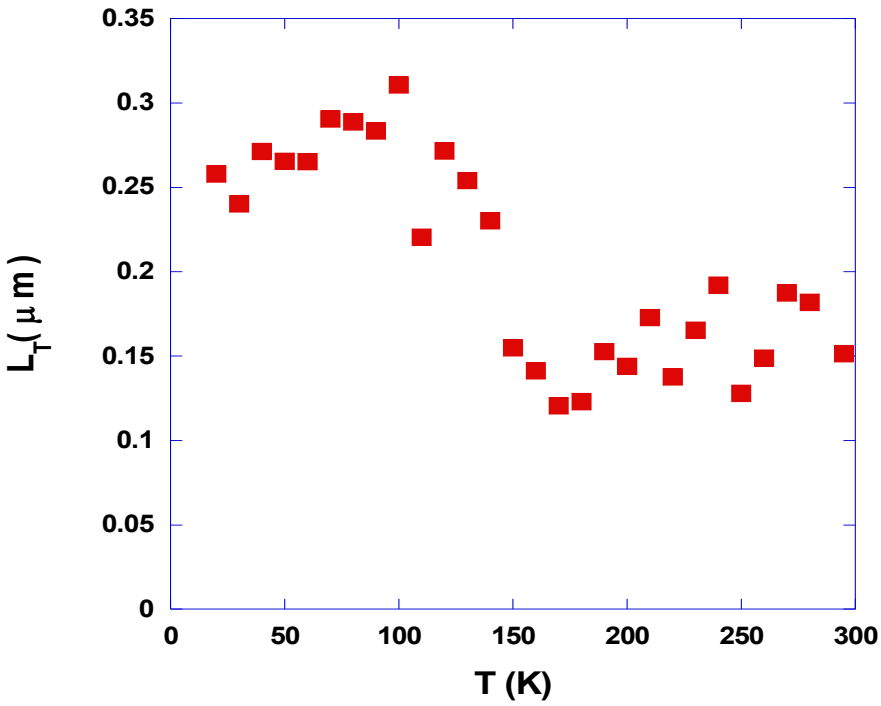

Figure 3.6 Variation of Lt as a function of temperature.

3.3 Other Factors that affect ARC

3.3.1 Non uniform contact interfaces

We measured the gaps (w) with field emission scanning electron microscope (FESEM). The outer parts of the gaps are not found uniform at GaMnAs and copper contact regions as shown in figure 3.7. Since the slope (i.e. the bulk GaMnAs contribution to the total resistance) is quite large, uncertainty in the width affects our result significantly. As the uniformity of the contact interfaces can't be controlled and the gap widths vary at the different parts of the feature. It is a major problem that creates apparent lack of reproducibility. This problem arises due to the limitation of the photolithography.

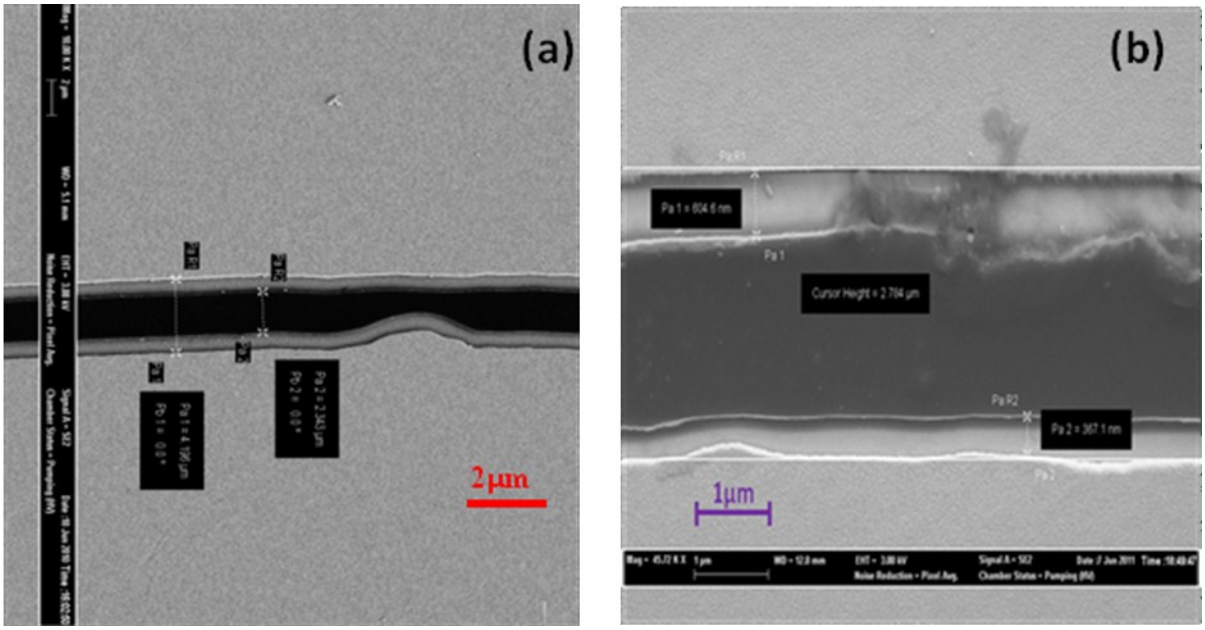

Figure 3.7 Contact edges as seen for (a) magnification×10K (b) magnification ×45.72K

The semiconductor gap varies at different parts of the circle. Some of the regions have narrow constrictions and the average value of the gap is deviated from the nominal width. Table 3.2 below shows the measured values of the gaps and their averages that are used to calculate the specific contact resistance. Figure 3.8 (a) shows the comparison of our result so obtained.

The gap widths (w) practically obtained are much different from the nominal values. For the features with smaller gap (3µm) the error is about 10%. This may introduce a significant change in specific contact resistance. Figure 3.8 (a) shows the change in contact resistance introduced due to this effect.

Table 3-2 Values of Semiconductor gaps (nominal and actual)

values of w (μm)	Measured values at different parts(μm)	Average value(μm)
3	2.784 ,2.74, 2.74	2.75
4	3.734, 3.61, 3.721, 3.615	3.67
6	5.66, 5.825, 5.745	5.74
8	7.614, 7.504, 7.593, 7.56	7.57
15	14.54, 14.62, 14.66, 14.54	14.59
20	19.34, 19.69,19.44, 19.59	19.51
40	39.55, 39.71, 39.60, 39.71	39.64
80	79.59, 79.58, 79.57	79.58

There is limitation of our device to get a uniform width of the semiconductor gaps. Care was taken minimizing the vibration during lithography. We turned off the blowers and any fans running inside the cleanroom when UV was exposed for making the patterns. The irregularities in the contact interfaces were incorporated taking the mean of the width in the diametrically opposite regions

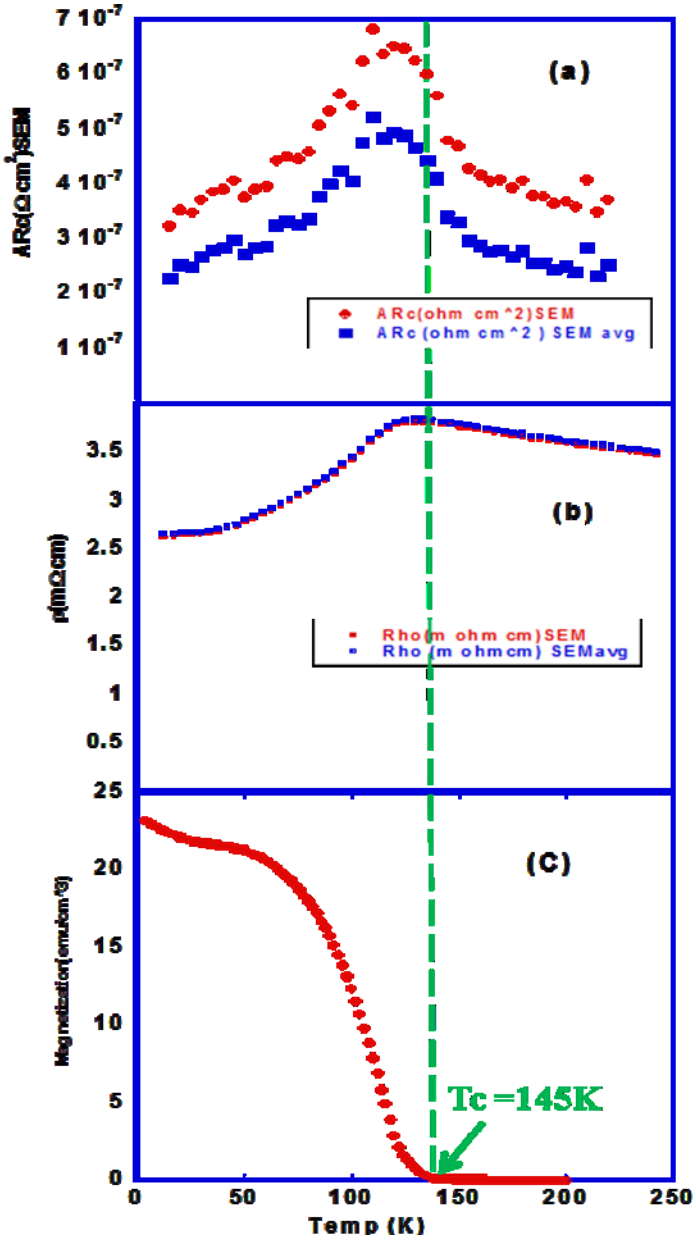

Figure 3.8 (a) ARc of GaMnAs as the function of temperature that that varies with gap w(b) Resistivity as the function of temperature (c) Variation of magnetization with temperature

We found that the value of ARc increases abruptly at Curie temperature due to its phase change from non magnetic to ferromagnetic. This is confirmed by the SQUID measurement of the sample. It was measured by Xinyu Liu at Notre Dame University,

Indiana. The result as seen in figure 3.8 (c) agrees with our result and shows the magnetization jumps up from zero at the Curie temperature (145 K in our case).

3.3.2 Oxides on the surface of the sample

The metal surface on the sample gets oxidized by atmospheric air as well as the ionized oxygen atoms during oxygen plasma etching. The oxide layer formed increases the resistivity of the metal that ultimately changes the specific contact resistance significantly. We measured that ARc for the two pieces of the same sample in the identical condition but removing oxide using the etching solution of mixture sulfuric acid and water (2:1000). We observed that value of ARc is about 1000 times larger for the sample with oxide on than the one with oxide removed. The variation of ARc with temperature is shown in figure

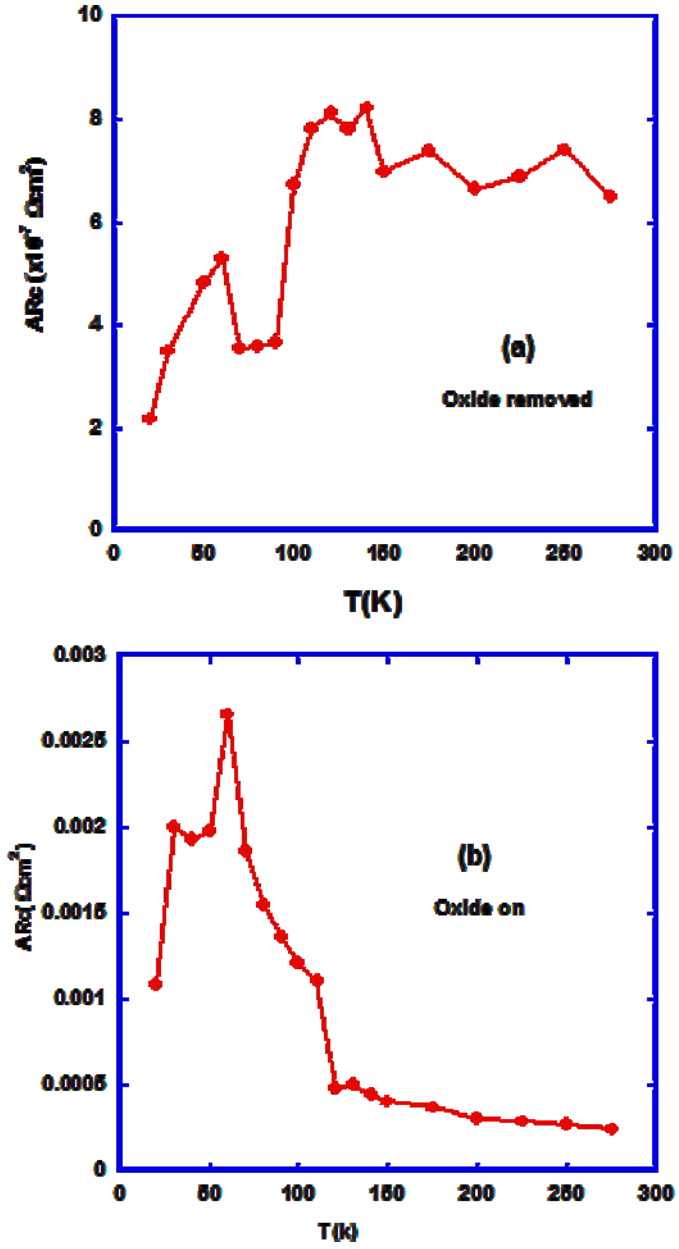

Figure 3.9 (a) ARc with oxide removed from the surface (b) ARc with oxide on the surface

3.3.3 Effect of annealing time

Specific contact resistance depends on resistivity of the contact materials. The value of resistivity for GaMnAs is a function of the impurities present in the sample. The impurities present in our sample are mainly the interstitial manganese atoms. This leads to an increase in resistivity since they act as double donors that compensate Ga[26]. Annealing the sample for longer time removes more interstitial Mn atoms and reduces the resistivity which ultimately decreases the specific contact resistance of the sample. Figure 3.10 displays the variation of ARc for the samples annealed for 1 hr and 92 hrs at 180°C. It is clear that ARc is higher for the sample annealed for less time.

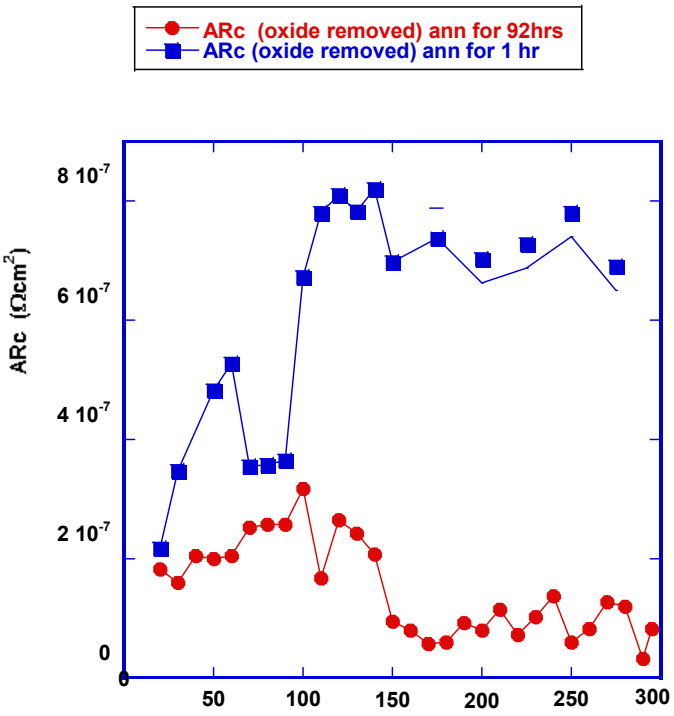

Figure 3.10 Comparison of ARc for samples annealed for different times

3.4 Confirmation of phase change of GaMnAs (Curie temperature)

Magnetic measurements are performed on each sample with a superconducting quantum interference device (SQUID) magnetometer. Figures 3.11 and 3.12 show the comparison of specific contact resistance, resistivity and magnetization as the function of temperature

dependent magnetization curves for the films in the annealed state with oxide on and oxide removed state. Results show that at the Curie temperature the magnetization of GaMnAs becomes zero that indicating that the sample has changed it phase and it switches its properties from paramagnetic to ferromagnetic or vice versa. It is seen that exactly at this temperature the specific contact resistance changes abruptly. Also the steepness of the resistivity is different at the two sides of the Curie temperature. The resistivity in figure 3.11 seems much rougher due to the oxide on the surface that causes resistivity non uniform.

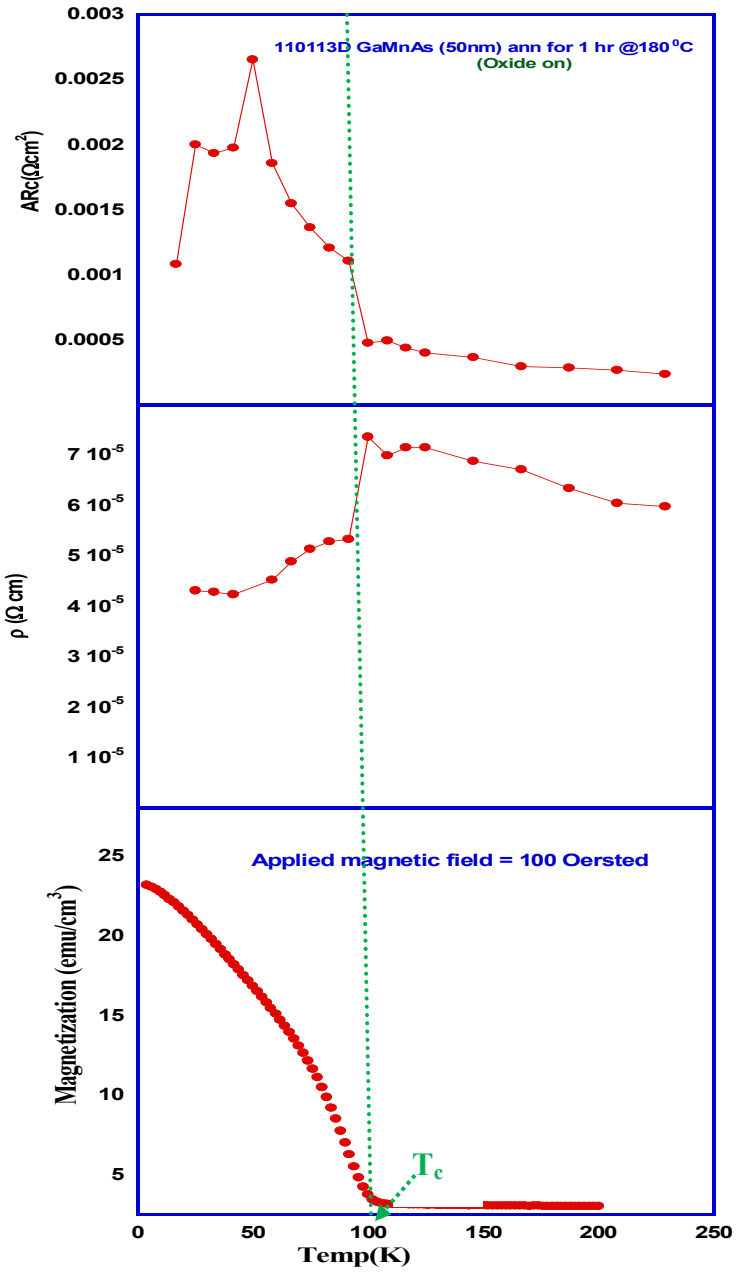

Figure 3.11 ARc, resistivity and magnetization of a sample with oxide on as the function of temperature

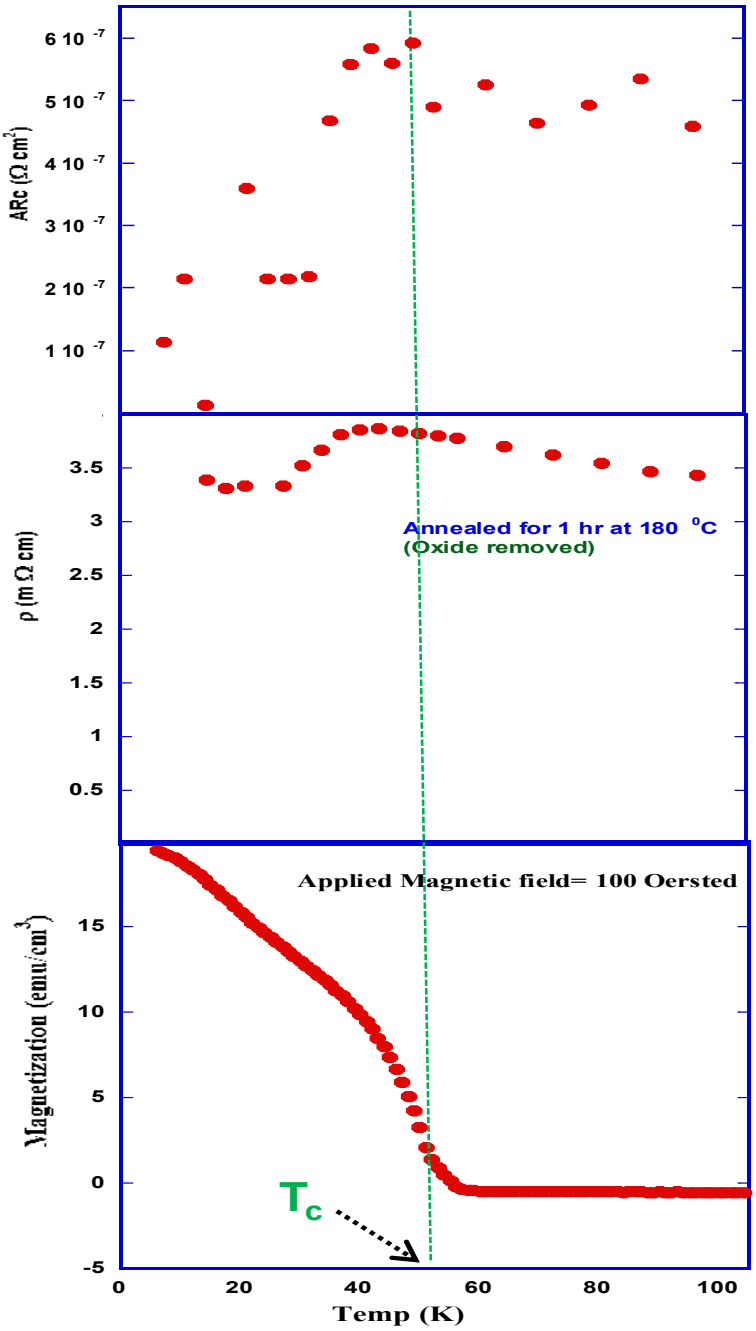

Figure 3.12 ARc, resistivity and magnetization of a sample with oxide removed as the function of temperature

The shift in the peak of AR has appeared at the Curie temperature towards lower temperature values. It might indicate that magnetization in the GaMnAs is suppressed near the Cu interface.

Chapter 4: CONCLUSION AND FUTURE WORK

This thesis is about experimental studies of magneto-transport in the ferromagnetic semiconductor GaMnAs. It is focused on measurement of specific contact resistance of the interface between GaMnAs and Copper using circular transmission line method.

We used annealed GaMnAs at 180K for 92hrs. The sample was fabricated by the method of photolithography. We measured the specific contact resistance in the interface between ferromagnetic semiconductor GaMnAs and non allyed Cu and found to be as low as $5\times10^{-8}\ \Omega cm^2$ with unstabilized. Our study shows that specific contact resistance increases abruptly up to the double of the value when the sample is cooled to Curie temperature at which GaMnAs becomes ferromagnetic. At the Curie temperature one of the two spin channels is suppressed due to phase transitions of GaMnAs that increases the resistance.

Future Work

Our work in specific contact resistance can be extended to study the specific contact resistance between GaMnAs and Niobium. Niobium becomes superconducting at cryogenic temperatures that are within our reach in a closed-cycle helium system. This enables us to study the transport properties in two regions.

1. Below and above the Curie temperature (Tc) where GaMnAs shows ferromagnetic orders transition.
2. Below and above 9K where Niobium shows superconducting phase transition.

Based on our results for GaMnAs interfaces we expect a large change in contact resistance at the region of Curie temperature for GaMnAs. We assume either spin up or spin down channels of conduction will get suppressed below Tc and specific contact resistance ARc decreases slowly with lowering temperature.

References

[1] N.W.Ashcroft and N.D.Mermin, Solid State Physics, 1st Edition (1976), Brooks Cole
[2] N.F. Mott, The Electrical Conuctivity of Transition metals, Proc. Roy. Soc.A153 (1936)699
[3] T. Valet and A. Fert, Phys. Rev. B**48**,7099 (1993)
[4] J. Bass, W. Pratt, Journal of Magnetism and Magnetic materials **200** (1999
[5] E.Hirota,H. Sakakima and K Inomata, Giant Magnetresistance Devices, Springer 2002
[6] M.Julliere, Tunelling between ferromagnetic films, Physics Letters**54**,3 (1975)
[7] A.A. Tulapurkar, Y. Suzuki, A. Fukushima, H. Kubota, H. Maehara et al., Spin-torque diode effect in magnetic tunnel junctions,Nature**438B**, 339-342(2005)
[8] Mark, C.Gould, L.W. Molenkamp et. al. , Phys. Rev. Lett. **103**, 017204 (2009)
[9] Pierre seneor, Anne Bernand-Mantel et al, Journal of Physics : Condensed Matter **19** (2007)
[10] F. Matsukrua, H. Ohno and T. Dieetl, III-V Ferromagnetic Semiconductors, Submitted to the Handbook of Magnetic materials (Ed, K. H. J. Bushcow) (Elsevier Science).
[11] K. Olejnik, M.S.H. Owen, V. Novak, J. Masek, A.C. Irvine et al.,Phys.Rev B**78** 054403(2008)
[12] D.K.Schroder, Semiconductor material and Device Characterization 3rd edition, John Wiley and sons, Inc, Hoboken, New Jersey(2006)
[13] L.J. Van der Pauw," A method of Measuring Specific Resistivity and Hall effect of Discs of Arbitary Shapr," Phil. Res.Rep.**13**,1-9, (1958)
[14] David J Sellmyer,Yi Liu, D. Shindo Handbook of Advanced Magnetic Materials, Volume IV Advanced Magnetic Materials: Properties and Applications, Tsinghua University Press
[15] E.Hirota,H.Sakakima and K Inomata,Giant Magnetoresistance Devices, Springer 2002
[16] F.A. Padovani and R. Stratton, "Field and Thermionic-Field Emission in Schottky Barriers",Solid-Staate Electron, **9**, 695-707, (1966)
[17]F.Braun "On the Current Transport in Metal Sulfides(in German)",Annal.Pys.Chem.**153**,556-563,1874
[18] W.Schottky, "Semiconductor Theory of Blocking Layer (in German)," *Naturwisenschaften***26**,843,1938
[19] Donald A Neaman, Semiconductor Pysics and Devices Basic Principles, 3rd Edition, Mc-Graw Hill (2002)
[20] P. Chen, J. Moser, P. Kotissek, J. Sadowski, M. Zenger, D. Weiss, and W. Wegscheider, Phys. Rev. **B 74**, 241302(R) (2006)
[21] G.K. Reeves, H.B. Harrison, "Obtaining the Specific Contact Resistance from Transmission Line Model Measurements" IEEE Electron Device Letters **3**,5 page 111 (1982)
[22] G.S. Marlow and M.B. Das, Solid State Electronics **25**, 91 (1982)
[23] M.Ahmad and B.M. Arora, "Investigation of AuGeNi Contacts Using Rectangular and Circular Transmission Line Model, Solid-State Electron,**35** , 14441-1445 (1992)
[24] G.S. Marlow and M.B. Das, " The Effects of Contact Size and Non-Zero metal Resistance on the Determination of Specific Contact Resistance, Solid-State Electronics,**25** 91-94 (1982)
[25] S.E. Swirhun and R.M. Swanson, IEEE Electron Device Letters **7**, 155 (1986)
[26] K.W. Edmonds, P. Boguslawski, K.Y. Wang, R.P. Campion, S.N. Novikov, N.R.S. Farley, B.L. Gallagher, C.T. Foxon, M. Sawicki, T. Dietl, M.B. Nardelli, and J. Bernholc, Phys. Rev. Lett. **92**, 037201 (2004)
[27] A. Einwanger, M. Ciorga,U. Wurstbauer, D. Schuh, W. Wegscheider, D.Weiss, Appl. Phys. Lett.**95**, 152101(2009)
[28] D. Chiba, M. Sawicki, Y. Nishitani, Y. Nakatani, F. Matsukura, and H. Ohno, Nature **455**, 515 (2008)
[29] K. Pappert, S. Humpfiner, C. Gould, J. Wenisch, K. Brunner, G. Schmidt, and L.W. Molenkamp, Nature Physics **3**, 573 (2007)
[30] K.A. Jones, E.H. Linifield , and J.E.F. Frost, Appl. Phys. Lett.**69**,4197(1996)
[31] T.V. Blank and Y.A. Gol'dberg, Semiconductors,**41**,1263(2007)